Optical and Quantum Electronics (2023) 55:1015
https://doi.org/10.1007/s11082-023-05282-x

A comprehensive first-principles study on the physical properties of Sr_2ScBiO_6 for low-cost energy technologies

Samah Al-Qaisi[1] · Habib Rached[2,3] · Malak Azmat Ali[4] · Zeesham Abbas[5] · Tahani A. Alrebdi[6] · Khaild I. Hussein[7] · Mohamed Khuili[8,9] · Nasir Rahman[10] · Ajay Singh Verma[11] · Mohammed Ezzeldien[12,13] · Manal Morsi[14,15]

Received: 12 June 2023 / Accepted: 7 August 2023 / Published online: 16 September 2023

Abstract
This paper presents a thorough first-principles investigation of the physical attributes of the double perovskite (DP) oxide, Sr_2ScBiO_6. The calculated lattice constant and the bond lengths adequately reflect the experimental data. In addition, the mBJ exchange potential analysis classified Sr_2ScBiO_6 as having a p-type semiconducting nature with an indirect bandgap value of 2.765 eV. Moreover, the mechanical properties analysis and the related elastic constants demonstrate the anisotropic nature of the Sr_2ScBiO_6 with decent mechanical stability. Apart from that, the Sr_2ScBiO_6 was considered a brittle non-central force solid with dominant covalent bondings. The varying optical parameter evaluations highlighted the potential use of Sr_2ScBiO_6 in visible-light (VIS) and ultraviolet (UV)-based optoelectronic devices. Furthermore, the semiconducting nature of Sr_2ScBiO_6 was verified through its thermoelectric response, which revealed that the charge carriers mostly consist of holes. The Sr_2ScBiO_6 recorded a high figure of merit (ZT) value, confirming that the material would be advantageous in renewable energy and thermoelectric (TE) applications.

Keywords Double perovskites · Transport properties · Solar cells · DFT · Renewable energy · Semiconductor

1 Introduction

In the past decades, the research community has shown a huge interest in perovskites, a class of materials comprising various mineral compounds. They have been exploited in numerous cutting-edge applications, including perovskite fuel cells, spintronics, and solid-oxide electrolyte fuel cells. Interestingly, double perovskites (DP) have demonstrated a significant role ahead of other materials, given their outstanding properties that are compatible with many industrial applications. In fact, DP oxides have been extensively employed in multiple fields, such as heterogeneous catalysts, thermoelectricity, transparent conductors, solar energy conversion, pigments, and photocatalysts (Xu et al. 2021; Nazir and Ikram 2022; Mishra et al. 2022; Rahman et al. 2022; Bidai et al. 2017; Moulay et al. 2015; Litimein et al. 2012).

Extended author information available on the last page of the article

More recently, greater attention has been focused on the development of DPs, particularly in the development of high-temperature thermoelectric devices (Roy et al. 2016; Saxena and Maiti 2018a, b). This corresponds to the rising demand for thermoelectric materials to minimize the over-reliance on the rapidly depleting fossil fuel sources. Realizing the exceptional performance of perovskite materials in thermoelectric applications, they have attracted global attention over their ability to transform waste heat into sound energy, which positions them as one of the promising open sources of green energy technologies (Song et al. 2022; Ali et al. 2021; Hu et al. 2021; Boudiaf et al. 2018).

One of the instruments used to assess the thermoelectric, optical, and electronic attributes of DP oxides is the Density Functional Theory (DFT). In one study, Aziz et al. (2022) evaluated the properties of X_2NaIO_6 (X = Pb, Sr) and revealed that both Sr_2NaIO_6 and Pb_2NaIO_6 exhibited good semiconducting behaviors with direct bandgaps (Eg) of 5.48 and 3.75 eV, respectively. In addition, Sr_2NaIO_6 achieved a higher ZT value and Power Factor (PF) of 0.7728 and 206.3, respectively. In addition, the cubic X_2NaIO_6(X = Pb, Sr) was more suitable in thermoelectric (TE) applications and optoelectronic devices (Aziz et al. 2022). In another study, Parrey et al. (2018) assessed the La_2NbMnO_6 DP. Based on the findings, La2NbMnO6 was suggested as having a half-metallic nature with an Eg of 3.75 eV. Moreover, the significant absorption of the entire infrared (IR) and ultraviolet (UV) spectra by La_2NbMnO_6 implies its potential application in UV and IR-based optoelectronic devices (Parrey et al. 2018). Furthermore, Rameshe et al. (2015) examined the physical properties of Sr_2AlNbO_6 and Sr_2AlTaO_6 in cubic symmetry. Several optical properties were calculated. Besides, the electronic structure was applied to determine the different Seebeck coefficients under various temperature conditions at varying carrier concentrations. According to the findings, the presence of a direct bandgap in both compounds indicates that both Sr_2AlNbO_6 and Sr_2AlTaO_6 were semiconducting materials (Rameshe et al. 2015). Meanwhile, Dar et al. (2019) reported that the semiconducting nature of Ba_2InTaO_6 was verified by the Seebeck coefficient (S) and its electrical conductivity (σ/τ), with electrons functioning as the main carriers. Thus, the study considered that the excellent PF of Ba_2InTaO_6 would be beneficial in thermoelectric devices (Dar et al. 2019). Additionally, Al-Qaisi et al. (2022a, 2022b) evaluated the thermoelectric properties of Ba_2NaIO_6 and Ba_2YBiO_6. The findings demonstrated that the Ba_2NaIO_6 and Ba_2YbiO_6 compounds were p-type semiconductors with direct and indirect bandgaps, respectively. The results also highlighted the potential of both compounds as base materials in thermoelectric and optoelectronic applications (Al-Qaisi et al. 2022a, b). Apart from that, Khandy et al. (2020) analysed the physical characteristics of Ba_2CdReO_6. The study found that the compound displayed a minimal stability energy curve in the ferromagnetic (FM) setup, while the half-metallic feature was observed in the band structure. Moreover, the physical attributes of the material were the major advantages that allowed it to be widely utilized as an electrode material in spintronics applications (Khandy et al. 2020).

In other studies, Hanif et al. (2022) explored the promising characteristics of Sr_2XNbO_6 (X = La, Lu) that could be implemented in the UV region of TE and optoelectronic devices. Both Sr_2LaNbO_6 and Sr_2LuNbO_6 exhibited direct bandgaps of 4.02 and 3.7 eV, respectively. Similarly, Haid et al. (2019) examined the optical properties of Sr_2CrTaO_6 and demonstrated the suitability of the compound in a broad range of visible light (VIS), UV, and IR-based applications. The Sr_2CrTaO_6 also exhibited a half-metallic ferrimagnetic ground state (Haid et al. 2019).

Based on the above literature, Sr_2ScBiO_6 is one of the promising members of the perovskite family that has not been fully explored in terms of its thermoelectric, electronic, structural, and optical attributes. Previously, Kazin et al. (2001a) evaluated the production and

crystalline structure of Sr_2ScBiO_6. High-resolution electron microscopy, and electron diffraction were utilized to analyze the crystal structure. Based on the results, the Sr_2ScBiO_6 was synthesized via a solid-state reaction technique in which the substance acquired the coveted oxygen stoichiometry at 850°C and remained stable up to 1150 °C. Regarding the structural features, Sr_2ScBiO_6 demonstrated a perovskite-derived rock-salt ordering of Bi^{5+} and Sc^{3+} on the *B* locations. In addition, the tolerance factor of the Sr_2ScBiO_6 was estimated to be 0.93 (Kazin et al. 2001a). In another study (Kazin et al. 2001b), Sr_2ScBiO_6 was prepared using oxides and carbonates through the nitrate route and compressed into a pellet. Subsequently, the pellet was burnt in a tubular furnace at 1050 °C for 72 h. The XRD analysis showed that the Sr_2ScBiO_6 was phase-pure and exhibited a Face-centered Cubic (FCC) structure with a lattice constant of 8.192 Å (Kazin et al. 2001b). Despite the available reports on this compound, there is a lack of efficient analysis of Sr_2ScBiO_6 via the most successful DFT approaches (Schwarz et al. 2002).

Meanwhile, the overwhelming demand for raw materials to satisfy the growing worldwide industrialization has outlined the urgent need to minimize global energy usage and explore alternative renewable energy sources. Concurrently, recent advance in quantum modelling and computing power has enabled researchers to perform accurate and efficient quantum mechanical calculations. This, in turn, provides the opportunity to extrapolate the calculating power such that even the previously complex properties of certain materials could now be identified and measured with pinpoint accuracy (Bowler 2016). Crystal structure of Sr_2ScBiO_6 has been discussed by XRD analysis which ensure the stability of this compound. The sintering of this double perovskite up to 1150 °C keep the structure which increase stability for practical applications (Kazin et al. 2001a). Furthermore, the changes in crystal structures with temperature strontium–bismuth-oxide system and their impact on practical applications had also been illustrated (Yang et al. 2018). The broad band NIR phosphor of Sr2ScSbO6: with Cr^{3+} ion doping has excellent thermal stability and high luminescence efficiency with external efficiency 82.0% at centered wavelength ~890 nm. This efficiency maintains up to 430K (Zhao et al. 2022). The researches probed the electronic, optical, magnetic, and thermoelectric properties of variety perovskites and double perovskites, e, g Khandy et al. explored the $Cs_2Ge(Mn/Ni)I_6$, $Ba_2(Er/Tb)NbO_6$, Cs_2GeMnX_6 (X = Cl, Br), and Ba_2XNbO_6 (X = Ho,Yb), for thermoelectric and spintronic applications (Shivhare et al. 2023; Khandy et al. 2023; Khandy and Gupta 2022, 2021a, b).

Therefore, this study aimed to perform a first-principle investigation of Sr_2ScBiO_6 DP as a potential low-cost material for renewable energy applications using the full potential DFT approach. This work involved the use of the generalized gradient approximation (GGA) (Perdew et al. 1996) and modified Becke–Johnson (mBJ) potential methods (Tran and Blaha 2009) to identify the thermoelectric, electronic, optical, and structural attributes of Sr_2ScBiO_6. Additionally, the BoltzTrap code (Madsen and Singh 2006) was utilized to determine the thermoelectric properties of the compound. It is expected that the present research will establish critical insights for future experimental and theoretical research.

2 Methods of calculation

This study employed the first-principle DFT-based full potential linearized augmented plane wave (FP-LAPW) scheme (Madsen et al. 2001) for the computation process following the WIEN2k package (Blaha et al. 2001), which is the ideal approach to determine the electronic features of solids (Muhammad et al. 2017; Al-Qaisi et al. 2020). The

Perdew–Burke–Ernzerhof (PBE) GGA version (PBE-GGA) was applied during the structural and elastic parameter calculations of the Sr_2ScBiO_6. Nevertheless, the PBE-GGA could only provide a precise measurement of the ground state under the energy bandgap values and structural properties of semiconductors (Perdew et al. 1996). Therefore, the Tran–Blaha modified Becke–Johnson exchange potential approximation (TB-mBJ) was performed to accurately project the material band structure (Tran and Blaha 2009). In the calculation, the muffin sphere radius (R_{MT}) as well as plane-wave cut-off (K_{max}) were set to 7, while the Gaussian factor (G_{max}) was held at 12. Afterwards, the R_{MT} values for the O, Bi, Sc, and Sr atoms were applied at 1.72, 2.1, 1.99, and 2.5 a.u, respectively. A mesh of $14\times14\times14$ and $50\times50\times50$ was also applied to compute the optoelectronic and transport evaluations, respectively. At 10^{-5} Ry, the convergence condition level was then met self-consistently. Subsequently, the results of the TB-mBJ band structure were computed to determine the thermoelectric and optical features of Sr_2ScBiO_6. Next, a dipole-matrix approach from the WIEN2k computational package was selected to further analyses the optical characteristics of Sr_2ScBiO_6 with an extended parameter value of 0.1 eV for the spectra. Ultimately, the Boltzmann transport equation was utilized to evaluate the thermoelectric characteristics of Sr_2ScBiO_6 following the semi-classical Boltzmann transport theory, as applied in the BoltzTrap code.

3 Results and discussion

3.1 Structural and elastic attributes of Sr_2ScBiO_6

The experimental lattice constant (a_{Exp}) was applied to determine the structural characteristics of Sr_2ScBiO_6, while the total energy of the crystal structure was reduced via Murnaghan's equation of states with respect to the unit cell volume (Murnaghan 1944). Table 1 presents the obtained ground structure according to several lattice parameters, such as the lattice constant (a), bulk modulus (B), and its pressure derivative ($B\prime$), as well as the lengths of the bonds between Sr–Bi, Bi–O, Sc–O, and Sr–O. Sr_2ScBiO_6 was crystallized with space group *Fm-3m* in an ideal cubic structure with an a_{Exp} value of 8.1895 Å (Kazin et al. 2001a, b). Furthermore, 8c (0.25, 0.25, 0.25), 4a (0, 0, 0), 4b (0.5, 0.5, 0.5), and 24e (0.2442, 0, 0) Wyckoff sites were coordinated by Sr, Bi, Sc and O, respectively. Interestingly, the optimized lattice constant (a) and bond lengths were close to the available experimental data (Kazin et al. 2001a, b), verifying the accuracy of the present computations. The optimization process and Sr_2ScBiO_6 crystal structure are shown in Fig. 1.

The elastic coefficients were calculated to determine the mechanical performance of the Sr_2ScBiO_6. Since it was revealed that the Sr_2ScBiO_6 exhibited a cubic crystalline structure, only the elastic parameters (C_{11},C_{12}, andC_{44}) were imperative for the mechanical characteristics analysis (Al-Qaisi et al. 2017). As summarized in Table 2, the elastic constants of the Sr_2ScBiO_6 in this study obeyed the mechanical stability criteria, including the "$C_{11}-C_{12}>0$, $C_{11}>0$, $C_{44}>0$, $C_{11}+2C_{12}>0$, C" (Khuili et al. 2023a). The elastic constants were used to derive other elastic parameters, including the Bulk (B) and Young (Y) moduli, Poisson's ratio (ν), as well as anisotropy factor (A), according to these expressions: $B=\frac{1}{3}\left(C_{11}+2C_{12}\right)$, $Y=\frac{9BG}{3B+G}$, $\nu=\frac{3B-2G}{2(3B+G)}$, and$A=\frac{2C_{44}}{C_{11}-C_{12}}$, where the shear modulus (G) refers to the material's response to the shear deformation (Al-Qaisi et al. 2017; Khuili et al. 2023a). The high bulk modulus value implies the remarkable strength of the Sr_2ScBiO_6 when subjected to external pressure. In addition, the low G of 79.58 GPa

Table 1 Comparison of the lattice constant a (Å), bulk modulus B (GPa), pressure derivative of the bulk modulus B′, bond lengths (Å), and energy bandgap Eg (eV) between the computed values and experimental values of Sr_2ScBiO_6

Sr_2ScBiO_6	a	B	B′	Sr–Bi	Bi–O	Sc–O	Sr–O	Eg using mBJ
Present	8.336	127.823	4.868	3.61	2.10	2.07	2.95	2.765
Others	Exp 8.189 (Kazin et al. 2001a), 8.192 (Kazin et al. 2001b) 8.297, 8.182 (Dimitrovska et al. 2005)	–	–	–	2.00(Kazin et al. 2001a)	2.095(Kazin et al. 2001a)	2.896(Kazin et al. 2001a)	–

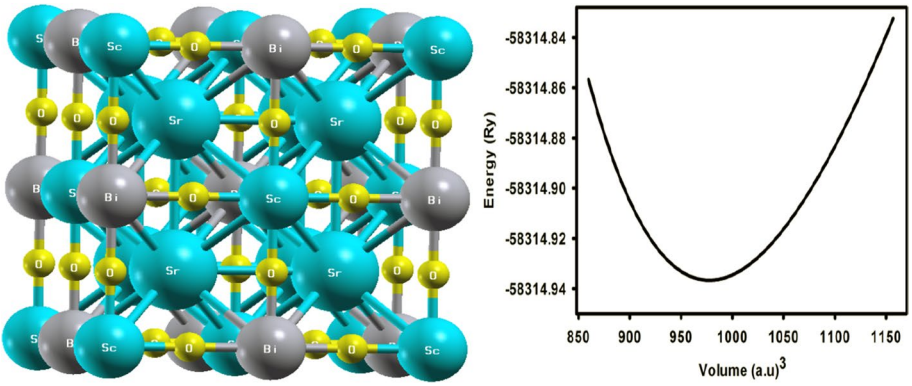

Fig. 1 The Sr_2ScBiO_6 crystal structure with a calculated total energy vs. volume plot

Table 2 The calculated elastic parameters of Sr2ScBiO6 based on the GGA-PBE approach

Sr_2ScBiO_6	C_{11} (GPa)	C_{12} (GPa)	C_{44} (GPa)	$C_{12}-C_{44}$ (GPa)	B (GPa)	G (GPa)	Y (GPa)	ν	A	B/G	T_m (K)
Value	258.32	61.51	69.02	-7.51	127.12	79.58	195.5	0.24	0.50	1.59	2079± 300

suggests a relatively smaller plastic twist in Sr_2ScBiO_6. Moreover, Young modulus (Y) refers to the stiffness of solids (Al-Qaisi et al. 2021a) in which a large Young's modulus value signifies a stronger resistance of the material against deformation. Therefore, the obtained Young's modulus value of the Sr_2ScBiO_6 indicates the degree of stiffness of the compound.

The Pugh's ratio (B/G) was measured to determine the brittleness/ductility of the Sr_2ScBiO_6. In general, a material is ductile when the B/G is over 1.75 and vice versa (< 1.75 = Brittle) (Pugh, S.: XCII. 1954; Alshahrani et al. 2020). Thus, the Sr_2ScBiO_6 was considered brittle in nature, given that the B/S ratio is lower than 1.75. Furthermore, Cauchy pressure (C_p) provides vital insights regarding the type of bonds and is represented by the following expression: $C_p = C_{12} - C_{44}$ (Pettifor 1992; Caid et al. 2023). Basically, a negative C_p value suggests a dominant presence of covalent bonds in the material, while a positive C_p value signifies that the material is composed mainly of ionic bonds. Based on the results, the Sr_2ScBiO_6 recorded a negative C_p value, confirming a dominant presence of covalent bonds in the compound. Like Pugh's ratio, Poisson's ratio (ν) classifies crystalline materials as brittle or ductile. A material is considered brittle or ductile depending on the separation line of $\nu = 0.26$ ($\nu < 0.26$ = Brittle; $\nu > 0.26$ = Ductile) (Vaitheeswaran et al. 2007). Table 2 indicates that the Poisson's ratio value of Sr_2ScBiO_6 is 0.241. Thus, the Sr_2ScBiO_6 crystal was classified as a brittle compound according to Poisson's ratio value, which was like the predicted Pugh's ratio. Apart from that, Poisson's ratio reflects the crystal's resistance to shearing force. A smaller Poisson ratio indicates that the material is more stable against shearing. In addition, a material is stable under a non-central or central force; based on Poisson's ratio, one may anticipate the nature of the force that contributes to the material's stability. Generally, a material with a Poisson's ratio of 0.25–0.50 is categorized as stabilized by the central force, termed a central force crystal. In contrast, a material that

possesses a Poisson's ratio beyond the fixed range is categorized as stabilized by the non-central force and is referred to as a non-central force crystal (Anderson and Demarest 1971; Al-Qaisi et al. 2023). Based on the findings, the Sr_2ScBiO_6 is a non-central crystal with a Poisson's ratio of 0.241.

The elastic anisotropy level was also evaluated based on the amount of deviation from unity. A Zener anisotropic factor A = 1 refers to isotropic materials (Al-Qaisi et al. 2023). According to the results in Table 2, the Sr_2ScBiO_6 was classified as anisotropic compound. The melting temperature was calculated based on the expression $T_m(K) = [553(K) \mp (5.911)C_{11}]$ GPa ∓ 300 K (Dar et al. 2019), which totalled 2079 ± 300 K.

Furthermore, the average elastic sound velocity, $v_m = \left[\frac{1}{3}\left(\frac{2}{v_t^3} + \frac{1}{v_l^3}\right)\right]^{-1/3}$, was calculated from the expression of longitudinal, $v_l = \left(\frac{B+\frac{4G}{3}}{\rho}\right)^{1/2}$, and the transverse velocities, $v_t = \left(\frac{G}{\rho}\right)^{1/2}$, while the Debye temperature, $\theta_D = \frac{h}{k_B}\left[\frac{3n}{4\pi}\left(\frac{N_A\rho}{M}\right)\right]^{1/3} v_m$, was measured to estimate the maximum possible temperature value of the crystal under the normal vibration model. The symbols N_A,k_B, h, and ρ, denote Avogadro's number, Boltzmann constant, Plank's constant, and density, respectively. (Wachter et al. 2001; Sun et al. 2004). The Debye temperature value also relates the elastic properties of solids to their thermodynamic features, such as vibrational entropy, melting point, and specific heat, making it an essential parameter of solids (Sun et al. 2004; Jasiukiewicz and Karpus 2003). Table 3 lists the results of the calculated parameters. The Sr_2ScBiO_6 recorded a high Debye temperature value of 492 K, which indicates the huge lattice thermal conductivity of the compound (Haque and Hossain 1802; Benkaddour et al. 2018). The Debye temperature also explains the hardness of solids, which is referred to as the Debye hardness (Arikan et al. 2020; Zhou et al. 2012). As shown in Table 3, the Sr_2ScBiO_6 has a high Debye hardness (492.46). Moreover, the calculated density value of Sr_2ScBiO_6, which equals 6.021 g/cm^3, is well agreed with the measured experimental value of 6.351 g/cm^3, as reported in past studies (Kazin et al. 2001a). The minimum lattice thermal conductivity has been computed whose ultralow values of ensure the importance of studied materials for thermoelectric and other applications.

3.2 Electronic attributes

It is vital to assess the energy band structure of materials to attain further insight into the respective material before it can be utilized in potential technological applications. Hence, the electronic energy band dispersion is used to categories materials into insulators, semiconductors, semi-metals, and metals. Given the successful use of the mBJ exchange potential in several past reports (Al-Qaisi et al. 2016; Reshak et al. 2012; Manzar et al. 2013), this study also employed the mBJ exchange potential to compensate for the underestimated

Table 3 The obtained results of density (ρ), Debye temperature (θ_D), Minimum Lattice thermal conductivity, transverse velocity (ν_t), longitudinal velocity (ν_l), and average sound velocity (v_m) for the Sr2ScBiO6 compound

Sr_2ScBiO_6	ρ(g/cm^3)	ν_t(m/s)	ν_l(m/s)	v_m(m/s)	κ_L (W/Km)	(θ_D) (K)
Value	6.021 Exp 6.351(Kazin et al. 2001a)	3653.67	6223.98	4032.07	0.080	492.46

gap (Dufek et al. 1994; Al-Qaisi et al. 2021b). Figure 2 presents the computed energy band structure of the Sr_2ScBiO_6 compound using the TB-mBJ approach. According to the TB-mBJ calculations in Table 1, the Sr_2ScBiO_6 exhibited an indirect bandgap of 2.765 eV between the minima of the conduction band (CB) at the X symmetry point and the maxima of the valence band (VB) at the Γ symmetry point.

A thorough investigation of the electronic structure was carried out by determining the total density of states (TDOS) and partial density of states (PDOS) spectra of the Sr_2ScBiO_6 using the TB-mBJ method between the −5 to 10 eV energy range, as shown in Figs. 2 and 3. The valence bands of the Sr_2ScBiO_6 were formed through the combination of the Sc-3*d*, Bi-5*d*, and O-2*p* orbitals within an energy range of −2.75 to −1.02 eV. Besides, the valence band group in the Sr_2ScBiO_6 between −4.3 and −2.93 eV were due to the Bi-6*p* and O-2*p* orbitals. As such, the valence band group was predominated by the O-2*p* states at a range of −0.94 eV to Fermi level. In contrast, the Bi-7*s* and Sc-3*d* states mainly dominated the lower conduction bands, with the O-2*p* states contributing a minor role. Overall, the Bi-6*p*, Sc-3*d*, and O-2*p* states in the unoccupied bands of the Sr_2ScBiO_6 resulted in an energy range of up to 6.05–9.96 eV.

3.3 Transport properties

The growing global energy consumption combined with the substantial energy loss through heat has forced the scientific community to seek novel materials and develop effective techniques to generate usable electrical energy from heat waste (Haq et al. 2021, 2022; Mahmood et al. 2022; Rached et al. 2022). Since the TB-mBJ approach estimates the exceptional energy bandgap value, the BoltzTrap code (Madsen and Singh 2006) was utilized to determine the thermoelectric properties of the Sr_2ScBiO_6 following the TB-mBJ band structure calculation. The thermoelectric aspects of the Sr_2ScBiO_6

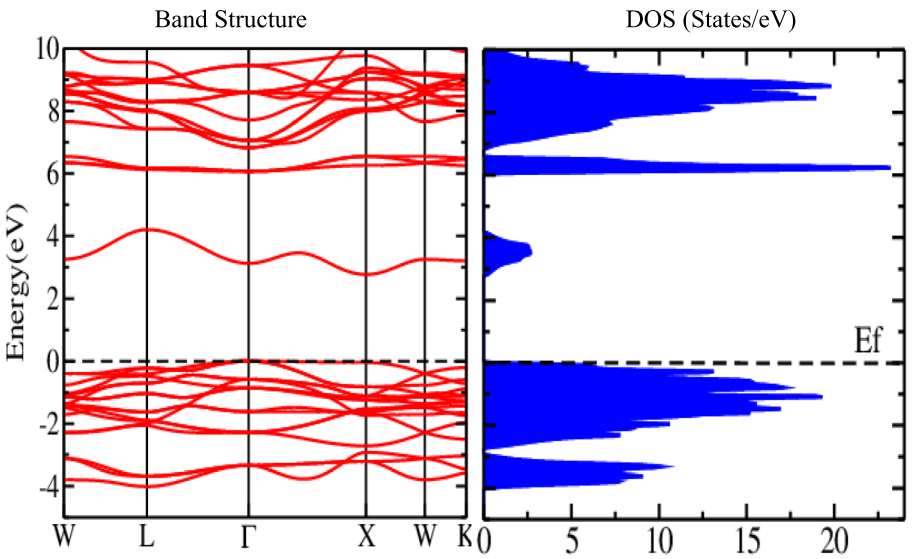

Fig. 2 The Sr_2ScBiO_6 band structure based on the TB-mBJ calculations

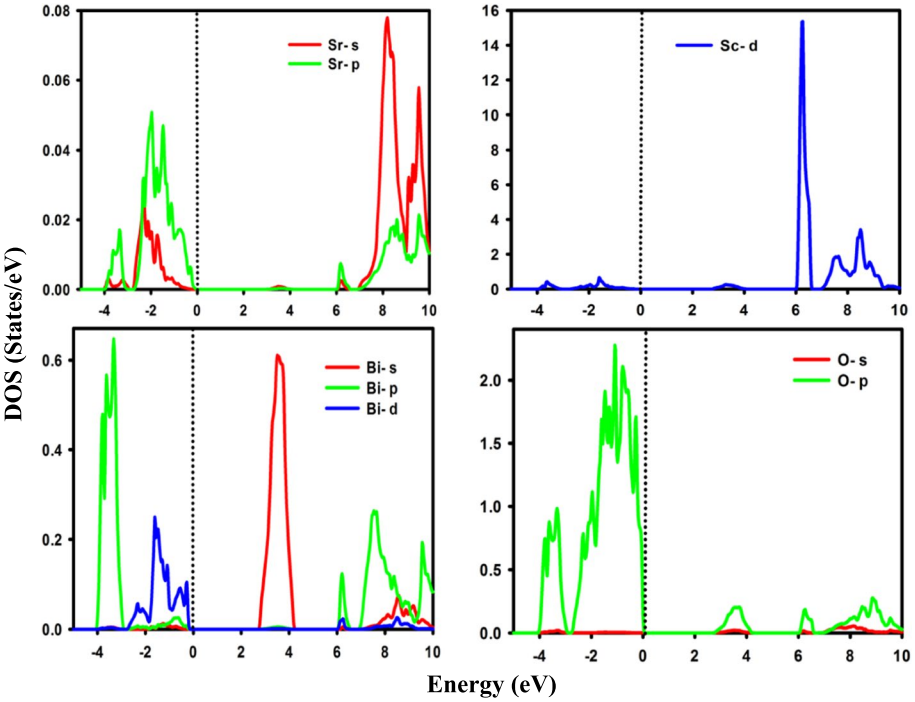

Fig. 3 The computed PDOS of the Sr_2ScBiO_6 compound based on the TB-mBJ method

DP were concisely analyzed in terms of the power factor ($PF = \sigma S^2/\tau$), thermal electronic conductivity (κ_e/τ), electrical conductivity (σ/τ), the figure of merit ($ZT = \sigma S^2/\kappa T$), and Seebeck coefficient (S) vs chemical potential (μ) at three varying temperatures of 300, 600, and 900 K (Figs. 4a–e). The dotted lines in each figure correspond to the Fermi level, which was presumed to be zero. Note that the μ is represented by a positive value for the n-type doping (electron-doped) region and a negative value for the p-type doping (hole-doped) region (Ali et al. 2023; Behera et al. 2023).

Based on Fig. 4a, Sr_2ScBiO_6 recorded a maximum S value in the electron-doped region at approximately 3020.16 μV/K at 300 K, as well as the lowest electrical conductivity value in the n-type doping region and declined when the temperature increased to 600 and 900 K. Additionally, at $\mu = 0$, the S value of the Sr_2ScBiO_6 was approximately 256.81 μV/K in which the positive value implies that the Sr_2ScBiO_6 compound is a p-type semiconductor with most of the charge carriers mainly consists of holes.

The plot of electrical conductivity (σ/τ) vs μ is shown in Fig. 4b. In terms of the energy bandgap, the material exhibited a low σ/τ in the μ range while a maximum σ/τ was achieved at higher μ values, corresponding to the p-type doping. In particular, the σ/τ rose to its highest value of 3.01×10^{20}/Ωms from zero at -0.65 eV in the hole-doped region. Accordingly, the σ/τ was influenced by the DOS or transport distribution function but unaffected by the temperature change. Thus, it was evidenced that the σ/τ of the Sr_2ScBiO_6 DP compound is temperature independent with an estimated σ/τ of 0.04×10^{20}/Ωms under room temperature conditions (300 K).

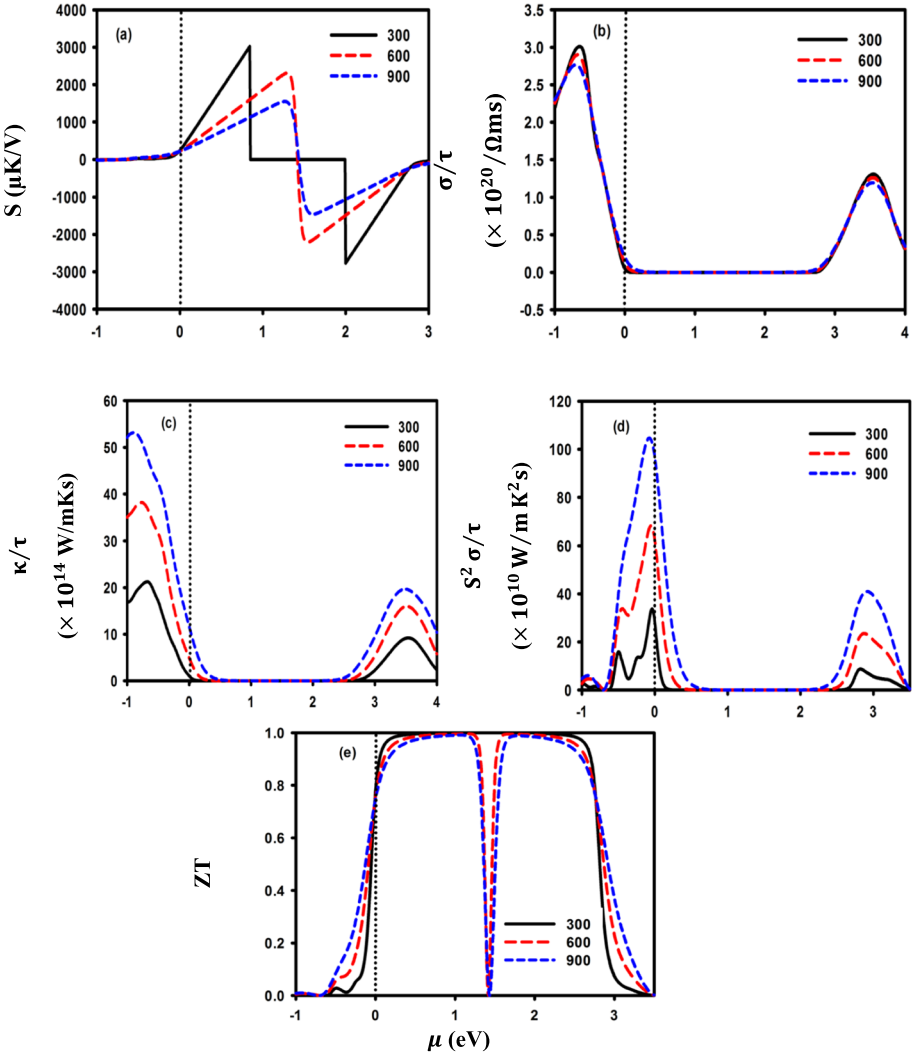

Fig. 4 The S, κ_e/τ, σ/τ, PF, and ZT of the Sr_2ScBiO_6 vs μ at various temperature levels

Comparable with the electronic conductivity (σ/τ), the electronic thermal conductivity (κ_e) of the Sr_2ScBiO_6 compound was detected in the hole-doped region, as portrayed in Fig. 4c. This was due to the connection between the κ_e value and the σ through the Wiedemann–Franz law, $\kappa_e = L\sigma T$, where L denotes the Lorentz number ($2.44 \times 10^{-8} J^2K^{-2}C^{-2}$ for free electrons) (Al-Qaisi et al. 2022c; Khuili et al. 2023b). The κ_e value corresponds to an increased temperature under a fixed pressure level. Here in our studied materials if thermal conductivity is multiplied with relaxation time (10^{-14}s) then the values of thermal conductivity becomes ultralow as compared to electrical conductivity. The κ/σ ratio becomes of the order of 10^{-6}. Therefore, the large values of Debye temperature and ultralow low values of thermal conductivity make them studied materials significantly important for thermoelectric applications. For the heat sensors and refrigerator applications, the materials should

have large values of electrical conductivity, and Seebeck coefficient with minimum thermal conductivity. Here in present results of thermoelectric properties, the ratio of κ/σ is very small of the order of 10^{-6} which shows the thermal conductivity relatively has ultralow value as compared to thermal conductivity. Therefore, the high values of power factor and figure of merit scale ensure significant of studied materials for electric generators, heat sensors, and refrigerators applications (Ashiq et al. 2023; Amin et al. 2022).

Furthermore, Fig. 4d depicts the plots of the PF of the Sr_2ScBiO_6 compound vs temperature. PF is typically used to determine the performance of a material to generate electricity. According to the figure, the p-type doping region of the compound recorded a significantly higher PF value compared to that of the n-type. The PF value increased with the temperature rise, and the maximum PF value of approximately 33.71×10^{10} W/mK^{2}s was achieved by the Sr_2ScBiO_6 compound at $\mu = -0.034$ under room temperature conditions (300 K).

The $ZT = S^2\ \sigma\ T/\kappa$ is considered the most crucial variable that determines the efficient performance of thermoelectric materials (Al-Muhimeed et al. 2022; Mustafa et al. 2022). ZT increases with the increase in electrical conductivity and S but decreases with the increment of κ. Figure 4e shows the ZT value of Sr_2ScBiO_6 as a function of μ. The Sr_2ScBiO_6 DP recorded several major peaks, with the maximum height measuring a ZT value of near 1 in the μ range, which corresponds to the highest S values, and rose with temperature. At the Fermi level, the Sr_2ScBiO_6 achieved a nearly consistent ZT value of 0.80 under different temperature effects. Hence, the high ZT value signifies the semiconducting nature of the Sr_2ScBiO_6 that would be advantageous in the development of thermoelectric technology.

3.4 Optical attributes

This section examines the interaction between the electromagnetic radiation of the Sr_2ScBiO_6 and its application in optoelectronics. Given that the dielectric function describes the interaction between the photons and electrons of a material, an insignificant wave vector portrays the linear response of the system to the incident light. The interaction is conveyed as a complex quantity following Cohen and Ehrenreich's equation: $\varepsilon(\omega) = \varepsilon_1(\omega) + i\,\varepsilon_2(\omega)$, where $\varepsilon_1(\omega)$ refers to the real component of the dielectric function ($\varepsilon(\omega)$) and is associated with anomalous dispersion and electronic polarization, and $\varepsilon_2(\omega)$ is defined as the imaginary component, which is related to the optical absorption of the solid (Maskar et al. 2021; Murtaza et al. 2021; Khuili et al. 2023c). In this study, the dielectric function, $\varepsilon(\omega)$ was analyzed to determine the response of the Sr_2ScBiO_6 to the incident light. The $\varepsilon_1(\omega)$ and $\varepsilon_2(\omega)$ were applied to compute the remaining optical parameters. Figure 5a–e present the optical variables of the computed equilibrium structure along with the incident energy of the radiation from 0 to 14 eV.

Figure 5a shows the real and imaginary components of the dielectric function, ($\varepsilon(\omega)$). The static value of $\varepsilon_1(\omega)$, particularly at $\varepsilon_1(0)$, is 3.12. The result in Fig. 5a also shows that the $\varepsilon_1(\omega)$ of Sr_2ScBiO_6 initially elevated with the increase in the incident electromagnetic radiation energy, subsequently generating two $\varepsilon_1(\omega)$ peaks at approximately 3.73 eV and 6.31 eV in the UV region. Afterwards, the $\varepsilon_1(\omega)$ declined swiftly and reached a negative value. Thus, the dielectric nature of the Sr_2ScBiO_6 demonstrated metallic properties when the $\varepsilon_1(\omega)$ accedes a negative value. Furthermore, Fig. 5a depicts that the threshold energy, $\varepsilon_2(\omega)$ of the Sr_2ScBiO_6 was approximately 2.763 eV, indicating the optical bandgap of the compound. The data was marginally close to the predicted energy bandgap of the

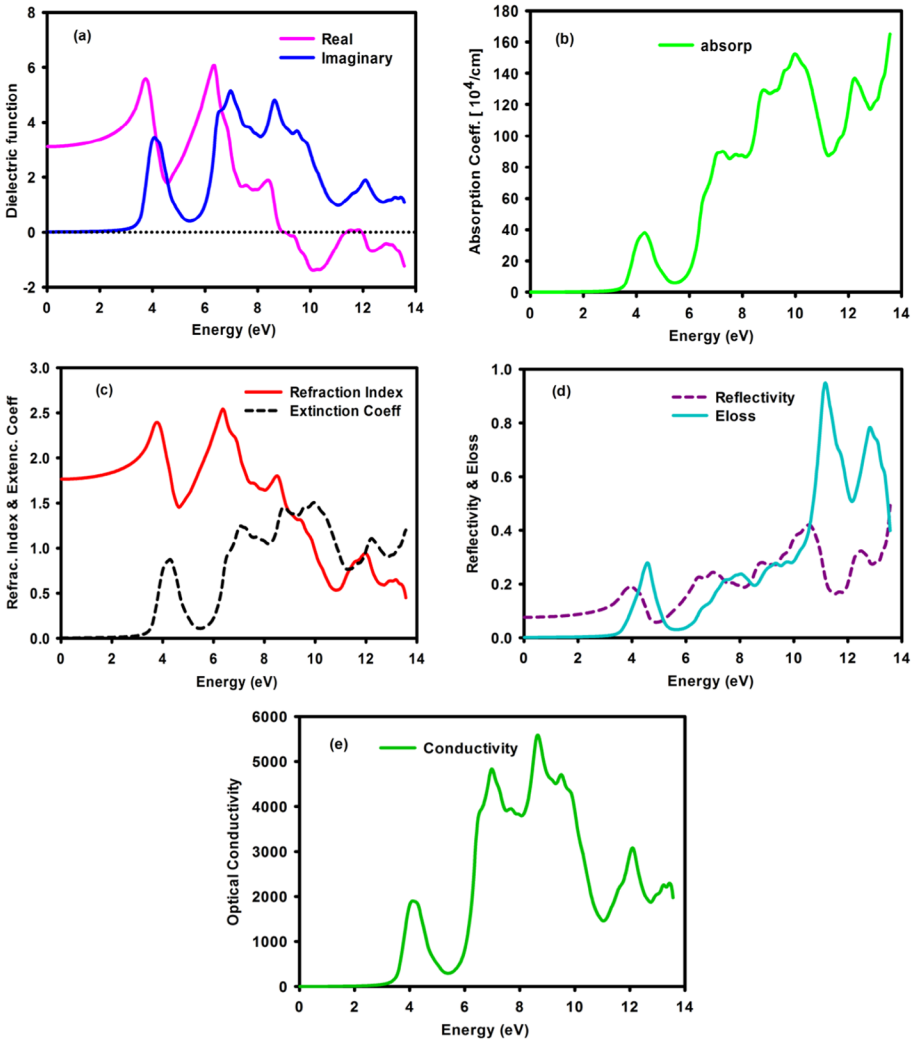

Fig. 5 Optical parameters of the Sr_2ScBiO_6 DP

electronic band structure (2.765 eV), demonstrating the extreme precision of the present findings. The optical transition between the maximum valence band (MVB) and the minimum conduction band (MCB) occurred at approximately 2.763 eV. Conversely, the curve accelerated beyond this point because of the sudden increment in the number of points that contributed to the $\varepsilon_2(\omega)$. Besides, two major peaks were detected in the Sr_2ScBiO_6 spectrum at 4.06 eV and 6.99 eV because of the electronic transition from the occupied O-2p state to the unoccupied Bi-6s state in the valence band.

Meanwhile, Fig. 5b presents the varying absorption coefficient, $\alpha(\omega)$ of the Sr_2ScBiO_6 as a function of the incident photon energy. In general, the α (ω) represents the absorbed amount of the incident light energy by the unit thickness of the material. A higher absorption coefficient value denotes that a material transports electron more efficiently from the VB to the CB (Rai et al. 2020; Albalawi et al. 2022). The results showed a wide range of

absorption regions from VIS to UV with a maximum α (ω) of 9.98 eV. In addition, the absorption edge of the Sr_2ScBiO_6 was 2.763 eV, which is in line with the indirect transition between the MCB and the MVB. Based on Fig. 5b, the $\alpha(\omega)$ was almost zero in the same region, where the optical conductivity, $\sigma(\omega)$ was also zero. The findings also revealed that the $\sigma(\omega)$ achieved a maximum value when the absorption reached its peak. Therefore, the outcome of this study demonstrated the suitability of the Sr_2ScBiO_6 in VIS and UV-based optoelectronic devices.

Additionally, Fig. 5c illustrates the n (ω), which is an optical factor that describes the penetration of light through a material and its absorption potential. When n (0), the static value of Sr_2ScBiO_6 was 1.77. As shown in the graph, the increase in n (ω) caused the energy of the incident radiation to increase, which peaked at 3.76 eV. However, the n (ω) spectrum declined drastically as photon energy increased until it reached the minimal value of less than 1 in the UV region. Moreover, the local maxima of the extinction coefficient, $K(\omega)$, of the Sr_2ScBiO_6 (Fig. 5c) was approximately 1.51 at 9.95 eV, which coincides with the zero value of $\varepsilon_1(\omega)$. According to Fig. 5a and c, it can be deduced that the n (ω) spectra correspond to the $\varepsilon_1(\omega)$ spectra.

The optical value, R (ω) of the Sr_2ScBiO_6 as a function of the incident radiation energy is portrayed in Fig. 5d. Based on the figure, the calculated zero-frequency R (0) of the Sr_2ScBiO_6 was 7.66%. The increment in the incident photon energy leads to the increased $R(\omega)$ value, which achieved a maximum value of approximately 42.14% in the UV region at 10.58 eV. Although the $R(\omega)$ fluctuated, the value remained minimum in the energy bandgap range. Overall, the transparency of the incident radiation energy up to the Eg demonstrates the promising properties of Sr_2ScBiO_6 in the production of lenses.

The results in Fig. 5d also present the calculated value of the electron loss function, $L(\omega)$. The plasma resonance properties were detected by the $L(\omega)$ peaks with a maximum resonant energy loss of 11.17 eV. In addition, Fig. 5e depicts the $\sigma(\omega)$ spectra of the incident radiation energy, which refers to the photoelectron's conduction under radiation energy. The $\sigma(\omega)$ of Sr_2ScBiO_6 began to increase beyond 2.76 eV and reached a maximum $\sigma(\omega)$ of 5544.45/Ωcm at 8.65 eV.

4 Conclusion

This study employed the DFT and Boltztrap calculations to explore the fundamental properties of the Sr_2ScBiO_6 DP. In terms of the structural and elastic characteristics, the Sr_2ScBiO_6 was essentially anisotropic and demonstrated good mechanical stability. Although the Sr_2ScBiO_6 compound was considered a brittle non-central force solid and composed mostly of covalent bonding, the energy volume plot produced a lattice constant that agrees with the results in past studies. Relating to the electronic properties, Sr_2ScBiO_6 was identified as an indirect bandgap of 2.765 eV with a p-type semiconducting nature. Furthermore, the optical properties of the Sr_2ScBiO_6 were predicted to provide an active response and beneficial impact for various applications in the VIS and UV range. Ultimately, the S, κ_e, PF, ZT, and σ of Sr_2ScBiO_6 were calculated with exceptional precision with substantial PF and ZT values, which is pivotal to achieving effective thermoelectric applications. It is worth noting that this is the first study that reports the thermoelectric properties of Sr_2ScBiO_6, which would serve as reference data to facilitate future studies.

Acknowledgements The author (Tahani A. Alrebdi) extends her sincere appreciation to Princess Nourah bint Abdulrahman University Researchers Supporting Project no. (PNURSP2023R71), Princess Nourah bint

Abdulrahman University, Riyadh, Saudi Arabia. The authors extend their appreciation to the Deanship of Scientific Research at King Khalid University, Saudi Arabia for funding this work through Large Groups Project under Grant no. L.R.G.P2/515/44.

Author contributions SA-Q, HR, MAA, ZA, TAA wrote the main manuscript. KIH, MK, NR prepared figures. ASV, ME, MM reviewed the manuscript.

Data availability Not applicable.

Code availability Not applicable.

Declarations

Conflict of interest No conflict of interests/competing interests.

Ethical approval Not applicable.

References

Albalawi, H., Nazir, G., Younas, M., Al-Qaisi, S., Ashiq, M., Alzahrani, J., Somaily, H., Morsi, M., Ghrib, T.: Study of lead-free vacancy ordered double perovskites Cs_2TeX_6 (X= Cl, Br, I) for solar cells, and renewable energy. Phys. Scr. **97**, 095801 (2022)

Ali, M.A., Reshak, A.H., Murtaza, G., AL-Anazy, M., Althib, H., Flemban, T.H., Bila, J.: Optoelectronic and transport properties of Rb/Cs_2TeI_6 defective perovskites for green energy applications. Int. J. Energy Res. **45**(6), 8448–8455 (2021)

Ali, M.A., Bahajjaj, A.A.A., Al-Qaisi, S., Sillanpää, M., Khan, A., Wang, X.: Structural, electronic, magnetic and thermoelectric properties of Tl_2NbX_6 (X= Cl, Br) variant perovskites calculated via density functional theory. J. Comput. Chem. (2023). https://doi.org/10.1002/jcc.27166

Al-Muhimeed, T.I., Alzahrani, J., Rouf, S.A., Al-Qaisi, S., Anbarasan, R., Mahmood, Q., Albalawi, H., Alharthi, S., Amin, M.A., Somaily, H.: Tuning of band gap by anion variation of Ga_2TiX_6 (X= Cl, Br, I) for solar cells and renewable energy. Phys. Scripta **97**, 085815 (2022)

Al-Qaisi, S., Abu-Jafar, M., Gopir, G.K., Khenata, R.: Electronic, structural and magnetic properties of TbO under pressure: FP-LAPW study. Phase Transit. **89**, 1155–1164 (2016)

Al-Qaisi, S., Abu-Jafar, M., Gopir, G.K., Ahmed, R., Omran, S.B., Jaradat, R., Dahliah, D., Khenata, R.: Structural, elastic, mechanical and thermodynamic properties of terbium oxide: first-principles investigations. Results Phys. **7**, 709–714 (2017)

Al-Qaisi, S., Ahmed, R., Ul Haq, B., Rai, D.P., Tahir, S.A.: A comprehensive first-principles computational study on the physical properties of lutetium aluminum perovskite $LuAlO_3$. Mater. Chem. Phys. **250**, 123148 (2020)

Al-Qaisi, S., Rai, D., Alshahrani, T., Ahmed, R., Haq, B.U., Tahir, S.A., Khuili, M., Mahmood, Q.: Structural, elastic, thermodynamic, electronic, optical and thermoelectric properties of $MgLu_2X_4$ (X= S, Se) spinel compounds from ab-initio calculations. Mater. Sci. Semicond. Process. **128**, 105766 (2021a)

Al-Qaisi, S., Rai, D., Haq, B.U., Ahmed, R., Vu, T.V., Khuili, M., Tahir, S.A., Alhashim, H.H.: First-principles investigation of structural, elastic, thermodynamic, electronic and optical properties of lead-free double perovskites halides: Cs_2LiYX_6 (X= Br, I). Mater. Chem. Phys. **258**, 123945 (2021b)

Al-Qaisi, S., Ali, M.A., Alrebdi, T.A., Vu, T.V., Morsi, M., Haq, B.U., Ahmed, R., Mahmood, Q., Tahir, S.A.: First-principles investigations of Ba2NaIO6 double Perovskite semiconductor: material for low-cost energy technologies. Mater. Chem. Phys. **275**, 125237 (2022a)

Al-Qaisi, S., Mushtaq, M., Alzahrani, J.S., Alkhaldi, H., Alrowaili, Z., Rached, H., Haq, B.U., Mahmood, Q., Al-Buriahi, M., Morsi, M.: First-principles calculations to investigate electronic, structural, optical, and thermoelectric properties of semiconducting double perovskite Ba_2YBiO_6. Micro Nanostruct. **170**, 207397 (2022b)

Al-Qaisi, S., Mushtaq, M., Alomairy, S., Vu, T.V., Rached, H., Haq, B.U., Mahmood, Q., Al-Buriahi, M.S.: First-principles investigations of Na_2CuMCl_6 (M = Bi, Sb) double perovskite semiconductors: materials for green technology. Mater. Sci. Semicond. Process. **150**, 106947 (2022c)

Al-Qaisi, S., Mebed, A.M., Mushtaq, M., Rai, D., Alrebdi, T.A., Sheikh, R.A., Rached, H., Ahmed, R., Faizan, M., Bouzgarrou, S.: A theoretical investigation of the lead-free double perovskites halides Rb_2XCl_6 (X= Se, Ti) for optoelectronic and thermoelectric applications. J. Comput. Chem. **44**, 1690–1703 (2023)

Alshahrani, T., Mustafa, G.M., Flemban, T.H., Althib, H., Al-Qaisi, S., Kattan, N.A., Mahmood, Q.: Probing of optoelectronic and transport properties of zinc based ZnY_2X_4 (X= S, Se) spinels for renewable energy. ECS J. Solid State Sci. Technol. **9**, 105001 (2020)

Amin, M.A., Nazir, G., Mahmood, Q., Alzahrani, J., Kattan, N.A., Mera, A., Mirza, H., Mezni, A., Refat, M.S., Gobouri, A.A.: Study of double perovskites X_2InSbO_6 (X= Sr, Ba) for renewable energy; alternative of organic-inorganic perovskites. J. Market. Res. **18**, 4403–4412 (2022)

Anderson, O.L., Demarest, H.H., Jr.: Elastic constants of the central force model for cubic structures: polycrystalline aggregates and instabilities. J. Geophys. Res. **76**, 1349–1369 (1971)

Arikan, N., Yildiz, G.D., Yildiz, Y.G., İyigör, A.: Electronic, elastic, vibrational and thermodynamic properties of HfIrX (X= As, Sb and Bi) compounds: insights from DFT-based computer simulation. J. Electron. Mater. **49**, 1–11 (2020)

Ashiq, M., Mahmood, Q., Zelai, T., Hakami, O., Kattan, N.A., Albalawi, H., Aljameel, A., Bouzgarrou, S., Ghrib, T., Hussein, K.I.: The narrow band bap double perovskites $X_2CuInCl_6$ (X= K, Rb, Cs) for optoelectronics, and thermoelectric applications. Mater. Sci. Eng. B **296**, 116690 (2023)

Aziz, A., Aldaghfag, S.A., Zahid, M., Iqbal, J., Yaseen, M., Somaily, H.: Theoretical investigation of X2NaIO6 (X= Pb, Sr) double perovskites for thermoelectric and optoelectronic applications. Phys. b: Condens. Matter **630**, 413694 (2022)

Behera, D., Mohammed, B., Taieb, S., Mokhtar, B., Al-Qaisi, S., Mukherjee, S.K.: First-principle investigations on optoelectronics and thermoelectric properties of lead-free Rb_2InSbX_6 (X= Cl, Br) double perovskites: for renewable energy applications. Eur. Phys. J. plus **138**, 520 (2023)

Benkaddour, Y., Abdelaoui, A., Yakoubi, A., Khachai, H., Al-Douri, Y., Omran, S.B., Shankar, A., Khenata, R., Voon, C.H., Prakash, D., Verma, K.D.: First-principle calculations of structural, elastic, and electronic properties of intermetallic rare earth R_2Ni_2Pb (R = Ho, Lu, and Sm) compounds. J. Supercond. Novel Magn. **31**, 395–403 (2018)

Bidai, K., Ameri, M., Amel, S., Ameri, I., Al-Douri, Y., Varshney, D., Voon, C.: First-principles calculations of pressure and temperature dependence of thermodynamic properties of anti-perovskite BiNBa3 compound. Chin. J. Phys. **55**, 2144–2155 (2017)

Blaha, P., Schwarz, K., Madsen, G.K., Kvasnicka, D., Luitz, J.: WIEN2K, An Augmented Plane Wave+ Local Orbitals Program for Calculating Crystal Properties, edited by K. Schwarz, Vienna University of Technology, Austria (2001)

Boudiaf, K., Bouhemadou, A., Al-Douri, Y., Khenata, R., Bin-Omran, S., Guechi, N.: Electronic and thermoelectric properties of the layered BaFAgCh (Ch= S, Se and Te): first-principles study. J. Alloy. Compd. **759**, 32–43 (2018)

Bowler, D.: Density functional theory: a tale of success in three codes. J. Phys.: Condens. Matter **28**, 421001 (2016)

Caid, M., Rached, D., Al-Qaisi, S., Rached, Y., Rached, H.: DFT calculations on physical properties of the lead-free halide-based double perovskite compound $Cs_2CdZnCl_6$. Solid State Commun. **369**, 115216 (2023)

Dar, S.A., Sharma, R., Srivastava, V., Sakalle, U.K.: Investigation on the electronic structure, optical, elastic, mechanical, thermodynamic and thermoelectric properties of wide band gap semiconductor double perovskite Ba_2InTaO_6. RSC Adv. **9**, 9522–9532 (2019)

Dimitrovska, S., Aleksovska, S., Kuzmanovski, I.: Prediction of the unit cell edge length of cubic A22+ BB′ O6 perovskites by multiple linear regression and artificial neural networks. Open Chem. **3**, 198–215 (2005)

Dufek, P., Blaha, P., Schwarz, K.: Applications of Engel and Vosko's generalized gradient approximation in solids. Phys. Rev. B **50**, 7279 (1994)

Haid, S., Benstaali, W., Abbad, A., Bouadjemi, B., Bentata, S., Aziz, Z.: Thermoelectric, structural, optoelectronic and magnetic properties of double perovskite Sr_2CrTaO_6: first principle study. Mater. Sci. Eng. B **245**, 68–74 (2019)

Hanif, A., Aldaghfag, S.A., Aziz, A., Yaseen, M., Murtaza, A.: Theoretical investigation of physical properties of Sr_2XNbO_6 (X= La, Lu) double perovskite oxides for optoelectronic and thermoelectric applications. Int. J. Energy Res. **46**, 10633–10643 (2022)

Haq, B.U., AlFaify, S., Al-shahrani, T., Al-Qaisi, S., Ahmed, R., Laref, A., Tahir, S.: First-principles investigations of ZnO monolayers derived from zinc-blende and 5–5 phases for advanced thermoelectric applications. J. Phys. Chem. Solids **149**, 109780 (2021)

Haq, B.U., AlFaify, S., Ahmed, R., Al-Qaisi, S., Alsardia, M., Khadka, I., Kim, S.-H.: Thermoelectric properties of different polymorphs of gallium phosphide: a first-priniciples study. Ceram. Int. **48**, 642–647 (2022)

Haque, E., Hossain, M.A.: High Seebeck coefficient and ultra-low lattice thermal conductivity in $Cs_2InAgCl_6$. arXiv preprint arXiv:1802.08136 (2018)

Hu, S., Ren, Z., Djurišić, A.B., Rogach, A.L.: Metal halide perovskites as emerging thermoelectric materials. ACS Energy Lett. **6**, 3882–3905 (2021)

Jasiukiewicz, C., Karpus, V.: Debye temperature of cubic crystals. Solid State Commun. **128**, 167–169 (2003)

Kazin, P., Abakumov, A., Zaytsev, D., Tretyakov, Y.D., Khasanova, N., Van Tendeloo, G., Jansen, M.: Synthesis and crystal structure of Sr_2ScBiO_6. J. Solid State Chem. **162**, 142–147 (2001a)

Kazin, P.E., Zaitsev, D.D., Tret'yakov, Y.D., Jansen, M.: Phase relations in the Bi–(Pb)–Sr–Ca–Cu–Sc–O System. Inorg. Mater. **37**, 1046–1050 (2001b)

Khandy, S.A., Gupta, D.C.: Intrinsic magnetism and thermoelectric applicability of novel halide perovskites Cs_2GeMnX_6 (X= Cl, Br): Route towards spintronics and energy harvesting technologies. Mater. Sci. Eng. B **265**, 114985 (2021a)

Khandy, S.A., Gupta, D.C.: Insight view of double perovskites Ba_2XNbO_6 (X= Ho, Yb) for spintronics and thermoelectric applications. Int. J. Energy Res. **45**, 13338–13354 (2021b)

Khandy, S.A., Gupta, D.C.: DFT analogue of prospecting the spin-polarised properties of layered perovskites Ba_2ErNbO_6 and Ba_2TmNbO_6 influenced by electronic structure. Sci. Rep. **12**, 19690 (2022)

Khandy, S.A., Yousuf, S., Bhat, T., Singh, S., Sofi, S., Mir, S., Seh, A.Q., Nabi, M., Ganie, N., Rasool, A.: Forecasting electronic-band structure and magnetism in complex double perovskite Ba_2CdReO_6. AIP Conf. Proc. **2265**, 030359 (2020)

Khandy, S.A., Alshahrani, T., Elsaeedy, H., Gupta, D.C.: First-principles calculations to investigate structural, electronic, phonon, magnetic and thermal properties of stable halide perovskite semiconductors Cs_2GeMnI_6 and Cs_2GeNiI_6. J. Alloy. Compd. **957**, 170296 (2023)

Khuili, M., Bounbaa, M., Fazouan, N., Abou Elmakarim, H., Sadiki, Y., Al-Qaisi, S., Allaoui, I., Maskar, E.H., Chahid, E.H., Maher, K., Abba, E.H.: First-principles study of structural, elastic, optoelectronic and thermoelectric properties of B-site-ordered quadruple perovskite $Ba_4Bi_3NaO1_2$. J. Solid State Chem. **322**, 123955 (2023a)

Khuili, M., Saadi, H., Fazouan, N., Sadiki, Y., Al-Qaisi, S., Atmani, E.H., Abba, E.H.: Study of the dependence of the ZT figure of merit on doping and temperature of ZnO. Int. J. Comput. Mater. Sci. Eng. **13**, 2350013 (2023b)

Khuili, M., El Hallani, G., Fazouan, N., Atmani, E., Allaoui, I., Al-Qaisi, S., Abba, E., Lekouch, K.: Experimental and theoretical studies of Mg-doped ZnO (Mg: ZnO) for optoelectronic applications. Int. J. Modern Phys. B **37**, 2350210 (2023c)

Litimein, F., Khenata, R., Bouhemadou, A., Al-Douri, Y., Omran, S.B.: First-principle calculations to investigate the elastic and thermodynamic properties of R BRh_3 (R= Sc, Y and La) perovskite compounds. Mol. Phys. **110**, 121–128 (2012)

Madsen, G.K., Singh, D.J.: BoltzTraP. A code for calculating band-structure dependent quantities. Comput. Phys. Commun. **175**, 67–71 (2006)

Madsen, G.K., Blaha, P., Schwarz, K., Sjöstedt, E., Nordström, L.: Efficient linearization of the augmented plane-wave method. Phys. Rev. B **64**, 195134 (2001)

Mahmood, Q., Nazir, G., Alzahrani, J., Kattan, N.A., Al-Qaisi, S., Albalawi, H., Mera, A., Mersal, G.A., Ibrahim, M.M., Amin, M.A.: Room temperature ferromagnetism and thermoelectric behavior of calcium based spinel chalcogenides CaZ2S4 (Z= Ti, V, Cr, Fe) for spintronic applications. J. Phys. Chem. Solids **167**, 110742 (2022)

Manzar, A., Murtaza, G., Khenata, R., Muhammad, S.: Electronic band structure and optical response of spinel SnX_2O_4 (X= Mg, Zn) through modified Becke–Johnson potential. Chin. Phys. Lett. **30**, 047401 (2013)

Maskar, E., Lamrani, A.F., Belaiche, M., Es-Smairi, A., Khuili, M., Al-Qaisi, S., Vu, T.V., Rai, D.: Electronic, magnetic, optical and transport properties of wurtzite-GaN doped with rare earth (RE= Pm, Sm, and Eu): First principles approach. Surfaces Interfaces **24**, 101051 (2021)

Mishra, S., Choudhary, R., Parida, S.: Structural, dielectric, electrical and optical properties of Li/Fe modified barium tungstate double perovskite for electronic devices. Ceram. Int. **48**, 17020–17033 (2022)

Moulay, N., Ameri, M., Azaz, Y., Zenati, A., Al-Douri, Y., Ameri, I.: Predictive study of structural, electronic, magnetic and thermodynamic properties of XFeO3 (X= Ag, Zr and Ru) multiferroic materials in cubic perovskite structure: first-principles calculations. Mater. Sci.-Pol. **33**, 402–413 (2015)

Muhammad, R., Shuai, Y., Tan, H.-P.: First-principles study on alkaline earth metal atom substituted monolayer boron nitride (BN). J. Mater. Chem. C **5**, 8112–8127 (2017)

Murnaghan, F.: The compressibility of media under extreme pressures. Proc. Natl. Acad. Sci. u.s.a. **30**, 244 (1944)

Murtaza, G., AlObaid, A.A., Al-Muhimeed, T.I., Al-Qaisi, S., Rehman, A., Hegazy, H., Nazir, G., Morsi, M., Mahmood, Q.: Tailoring of band gap to tune the optical and thermoelectric properties of Sr_1-xBaxSnO$_3$ stannates for clean energy; probed by DFT. Chem. Phys. **551**, 111322 (2021)

Mustafa, G.M., Hassan, M., Aloufi, N.M., Saba, S., Al-Qaisi, S., Mahmood, Q., Albalawi, H., Bouzgarrou, S., Somaily, H., Mera, A.: Half metallic ferroamgnetism, and transport properties of vacancy ordered double perovskites Rb_2 (Os/Ir) X_6 (X= Cl, Br) for spintronic applications. Ceram. Int. **48**, 23460–23467 (2022)

Nazir, N., Ikram, M.: Tuning of the structural, morphological, dielectric, and magnetoresistance properties of Gd2NiMnO6 double perovskite by Ca doping. Physica B **632**, 413734 (2022)

Parrey, K.A., Khandy, S.A., Islam, I., Laref, A., Gupta, D.C., Niazi, A., Aziz, A., Ansari, S., Khenata, R., Rubab, S.: Electronic structure, optical and transport properties of double perovskite La_2NbMnO_6: a theoretical understanding from DFT calculations. J. Electron. Mater. **47**, 3615–3621 (2018)

Perdew, J.P., Burke, K., Ernzerhof, M.: Generalized gradient approximation made simple. Phys. Rev. Lett. **77**, 3865 (1996)

Pettifor, D.: Theoretical predictions of structure and related properties of intermetallics. Mater. Sci. Technol. **8**, 345–349 (1992)

Pugh, S.: XCII. Relations between the elastic moduli and the plastic properties of polycrystalline pure metals. London Edinb. Dublin Philos. Magaz. J. Sci. **45**, 823–843 (1954)

Rached, Y., Caid, M., Rached, H., Merabet, M., Benalia, S., Al-Qaisi, S., Djoudi, L., Rached, D.: Theoretical insight into the stability, magneto-electronic and thermoelectric properties of XCrSb (X: Fe, Ni) half-Heusler alloys and their superlattices. J. Supercond. Novel Magn. **35**, 875–887 (2022)

Rahman, A.U., Aurangzeb, M., Khan, R., Zhang, Q., Dahshan, A.: Predicted double perovskite material Ca_2ZrTiO_6 with enhanced n-type thermoelectric performance. J. Solid State Chem. **305**, 122661 (2022)

Rai, D., Laref, A., Khuili, M., Al-Qaisi, S., Vu, T.V., Vo, D.D.: Electronic, magnetic and optical properties of monolayer (ML) hexagonal ZnSe on vacancy defects at Zn sites from DFT-1/2 approach. Vacuum **182**, 109597 (2020)

Rameshe, B., Rajagopalan, M., Palanivel, B.: Electronic structure, structural phase stability, optical and thermoelectric properties of Sr_2AlM'O6 (M'= Nb and Ta) from first principle calculations. Comput. Condens. Matter **4**, 13–22 (2015)

Reshak, A.H., Auluck, S., Piasecki, M., Myronchuk, G., Parasyuk, O., Kityk, I., Kamarudin, H.: Absorption and photoconductivity spectra of Ag_2GeS_3 crystal: experiment and theory. Spectrochim. Acta Part A Mol. Biomol. Spectrosc. **93**, 274–279 (2012)

Roy, P., Bose, I., Maiti, T.: Synthesis and characterization of Sr2TiMO6 (M= Fe, Co) double perovskites for high temperature thermoelectric applications. Integr. Ferroelectr. **174**, 34–42 (2016)

Saxena, M., Maiti, T.: Compositional modification of Sr2TiCoO6 double perovskites by Mo and La for high temperature thermoelectric applications. Ceram. Int. **44**, 2732–2737 (2018a)

Saxena, M., Maiti, T.: Evaluation of Ba doped $Sr_2TiFe_{0.5}Mo_{0.5}O_6$ double perovskites for high temperature thermoelectric power generation. Scripta Mater. **155**, 85–88 (2018b)

Schwarz, K., Blaha, P., Madsen, G.K.: Electronic structure calculations of solids using the WIEN2k package for material sciences. Comput. Phys. Commun. **147**, 71–76 (2002)

Shivhare, V., Khandy, S.A., Gupta, D.C.: Probing the structural, mechanical, phonon, thermal, and transport properties of magnetic halide perovskites $XTiBr_3$ (X= Rb, Cs) through ab-initio results. Sci. Rep. **13**, 9115 (2023)

Song, X., Shai, X., Deng, S., Wang, J., Li, J., Ma, X., Li, X., Wei, T., Ren, W., Gao, L.: Anisotropic chalcogenide perovskite $CaZrS_3$: a promising thermoelectric material. J. Phys. Chem. C **126**, 11751–11760 (2022)

Sun, Z., Li, S., Ahuja, R., Schneider, J.M.: Calculated elastic properties of M_2AlC (M= Ti, V, Cr, Nb and Ta). Solid State Commun. **129**, 589–592 (2004)

Tran, F., Blaha, P.: Accurate band gaps of semiconductors and insulators with a semilocal exchange-correlation potential. Phys. Rev. Lett. **102**, 226401 (2009)

Vaitheeswaran, G., Kanchana, V., Svane, A., Delin, A.: Elastic properties of $MgCNi_3$—a superconducting perovskite. J. Phys.: Condens. Matter **19**, 326214 (2007)

Wachter, P., Filzmoser, M., Rebizant, J.: Electronic and elastic properties of the light actinide tellurides. Physica B **293**, 199–223 (2001)

Xu, X., Xu, Y., Ma, J., Yin, Y., Fronzi, M., Wang, X., Bi, L.: Tailoring electronic structure of perovskite cathode for proton-conducting solid oxide fuel cells with high performance. J. Power Sources **489**, 229486 (2021)

Yang, Y., Li, J., Yuan, Y., Pan, F., Shi, D., Lin, C., Du, X., Sun, J.: Synthesis and crystal structure of $Sr_3Bi_2O_6$ and structural change in the strontium–bismuth-oxide system. Dalton Trans. **47**, 1888–1894 (2018)

Zhao, M., Liu, S., Cai, H., Zhao, F., Song, Z., Liu, Q.: Efficient broadband near-infrared phosphor Sr_2ScSbO_6: Cr^{3+} for solar-like lighting. Sci. China Mater. **65**, 748–756 (2022)

Zhou, D., Liu, J., Xu, S., Peng, P.: Thermal stability and elastic properties of Mg_2X (X= Si, Ge, Sn, Pb) phases from first-principle calculations. Comput. Mater. Sci. **51**, 409–414 (2012)

Authors and Affiliations

Samah Al-Qaisi[1] · Habib Rached[2,3] · Malak Azmat Ali[4] · Zeesham Abbas[5] · Tahani A. Alrebdi[6] · Khaild I. Hussein[7] · Mohamed Khuili[8,9] · Nasir Rahman[10] · Ajay Singh Verma[11] · Mohammed Ezzeldien[12,13] · Manal Morsi[14,15]

✉ Samah Al-Qaisi
samah.qaisi@gmail.com

✉ Tahani A. Alrebdi
taalrebdi@pnu.edu.sa

Habib Rached
habib.rached@gmail.com

Malak Azmat Ali
azmatupesh@gmail.com

Zeesham Abbas
zeeshamabbas035@gmail.com

Khaild I. Hussein
imed_boukhris@yahoo.fr

Mohamed Khuili
m.khuili@usms.ma

Nasir Rahman
nasir@ulm.edu.pk

Ajay Singh Verma
drajayphy@gmail.com

Mohammed Ezzeldien
meabas@ju.edu.sa

Manal Morsi
m.mahd@psau.edu.sa

[1] Palestinian Ministry of Education and Higher Education, Nablus, Palestine

[2] Faculty of Exact Sciences and Informatics, Department of Physics, Hassiba Benbouali University of Chlef, Ould-Fares, Chlef, Algeria

[3] Magnetic Materials Laboratory, Department of Materials and sustainable development, Faculty of Exact Sciences, Djillali Liabes University of Sidi Bel-Abbes, Djillali Liabes, Algeria

[4] Department of Physics, Government Post Graduate Jahanzeb College Saidu Sharif, Swat 19130, Khyber Pakhtunkhwa, Pakistan

[5] Department of Nanotechnology and Advanced Materials Engineering, Sejong University, Seoul, Republic of Korea

[6] Department of Physics, College of Science, Princess Nourah Bint Abdulrahman University, Riyadh, Saudi Arabia

[7] Department of Radiological Sciences, College of Applied Medical Sciences, King Khalid University, 61421 Abha, Saudi Arabia

[8] CRMEF of Beni Mellal-Khénifra, Beni-Mellal, Morocco

[9] Superior School of Technology (EST-Khenifra), University of Sultan Moulay Slimane, PB 170, 54000 Khenifra, Morocco

[10] Department of Physics, University of Lakki Marwat, Lakki Marwat 28420, Khyber Pukhtunkhwa, Pakistan

[11] Division of Research and Innovation, School of Applied and Life Sciences, Uttaranchal University, Dehradun 248007, India

[12] Physics Department, College of Science, Jouf University, Al-Jouf, P.O. Box 2014, Sakaka, Saudi Arabia

[13] Metallurgy and Material Science Tests (MMST) Lab, Department of Physics, Faculty of Science, South Valley University, Qena, Egypt

[14] Department of Physics, College of Arts and Science, Prince Sattam Bin Abdulaziz University, Wadi Addawasir, Saudi Arabia

[15] Department of Physics, Girl College for Art, Science, and Education, Ain-Shams University, Cairo, Egypt